Pulling Helices inside Bacteria: Imperfect Helices and Rings

Jun F. Allard
Institute of Applied Mathematics, University of British Columbia, Vancouver, British Columbia, Canada, V6T 1Z2

Andrew D. Rutenberg*
Department of Physics and Atmospheric Science, Dalhousie University, Halifax, Nova Scotia, Canada, B3H 3J5

(Received 17 November 2008; published 17 April 2009)

We study steady-state configurations of intrinsically-straight elastic filaments constrained within rod-shaped bacteria that have applied forces distributed along their length. Perfect steady-state helices result from axial or azimuthal forces applied at filament ends, however azimuthal forces are required for the small pitches observed for MreB filaments within bacteria. Helix-like configurations can result from distributed forces, including coexistence between rings and imperfect helices. Levels of expression and/or bundling of the polymeric protein could mediate this coexistence.

DOI: 10.1103/PhysRevLett.102.158105 PACS numbers: 87.16.Ln, 87.16.A−

Many components of the prokaryotic cytoskeleton [1,2] exhibit helical configurations within rod-shaped bacteria such as *Escherichia coli*. For example, the tubulin homolog FtsZ can exhibit helices [3], while the actin homolog MreB generically exhibits helices [4]. Other polymerizing filaments also exhibit helices within bacteria, such as MinD, ParA, and the RNA degradosome [5]. Helical localization patterns have also been reported in peptidoglycan synthesis [6]. New helically localized proteins continue to emerge, see e.g. [7]. Formation mechanisms have not been demonstrated for any of these helices. A detailed understanding of helical formation mechanisms within bacteria, and understanding how to manipulate them, will help to dissect their significance within bacteria. While helices in free space have been well studied [8], we must also understand the confining effects of a cylindrical bacterial shape.

Equilibrium helices could arise from intrinsically curved elastic filaments and/or a curved bacterial membrane with strongly anisotropic interactions between filaments and the membrane [9]. Polymeric filaments of FtsZ do exhibit small (intrinsically curved) loops both *in vitro* and in the cytoplasm of rod-shaped fission yeast [10]. However, other polymeric filaments do not appear to have intrinsic curvature, such as MreB, which exhibits straight filaments when expressed within fission yeast [11]. Furthermore, it is not known how anisotropic the interactions between filaments and membranes actually are.

For filaments without either intrinsic curvature or anisotropic membrane interactions, the simplest explanation of helices in rod-shaped bacteria is the locally-straight polymerization (''shooting'') from a randomly oriented nucleus [2]. For rod-shaped bacteria, a randomly oriented nucleus on the cell's lateral wall making an angle θ with the cell's axis would extend into a helix with a pitch $p = 2\pi R/\tan\theta$, where R is the cell radius. By transforming a uniform distribution for θ, the pitch p will have a distribution

$$g(p) = 4R/(p^2 + 4\pi^2 R^2). \quad (1)$$

This distribution is broad: its mean and variance both diverge. If the nucleus is randomly oriented in the hemispherical end caps, the distribution will be biased towards even longer pitches and still with a divergent width. Any relaxation of an intrinsically-straight filament would also bias the distribution towards longer pitches that have lower elastic energies [12]. However, reported bacterial helices do not appear to have pitches that are so long and so broadly distributed. Randomly oriented filaments also cannot explain the distinctive coexistence of rings and helices within extended filaments, as seen with MreB in *E. coli* [13].

MreB is an actinlike protein that is found in all rod-shaped bacteria [6]. MreB directs lateral cell wall synthesis and localizes several proteins to the bacterial cell poles [4,14]. It appears in a variety of configurations, including helices running the length of the cylindrical portion of *Caulobacter crescentus* and *Bacillus subtilis*, rings in *Rhodobacter sphaeroides* and spherical mutants of *E. coli* [15]; and rings and/or helices in *E. coli* [13].

From its apparent thickness and homology with eukaryotic actin, MreB filaments have bending stiffness less than the bacterial cell wall ($B \sim 10^5$ pN nm^2), and a persistence length larger than the bacterial cell size ($\xi \sim 10$–100 μm) [16]. Thus, cell shape should provide significant constraints to straight filaments. Indeed, MreB structures are found close to the membrane [2,4,13]. Their affinity for the membrane appears to be indirect, through interaction with transmembrane proteins MreC and MreD [14,15]. It seems likely that such indirect affinity for the membrane would be at most weakly anisotropic. Accordingly, in this Letter we restrict the filament to the membrane and do not impose twist forces [9,17].

External forces could act on intrinsically-straight MreB filaments. RNA polymerase can generate forces up to 25 pN, is present in bacteria, and interacts with MreB [18]. Cell wall synthesis machinery is thought to rotate around the circumference of the cell as it inserts peptido-

glycan [19], requires MreB or its homologs for normal functioning in various cells [6,15,20], and could pull azimuthally on the MreB helix. Polymerization forces may also act on filaments [21]. We explore how such nonconstraint forces, i.e., forces other than the constraint forces holding it to the cylindrical cell wall, can lead to helixlike shapes within rod-shaped cells.

We compute the equilibrium configuration of an inextensible but flexible filament of length L constrained to lie on a cylinder of radius R. In agreement with experiment in *B. subtilis* [22] and consistent with most MreB configurations seen in *E. coli* [13], we only consider the helix within the cylindrical part of the cell. The elastic energy density is $\mathcal{H}_0 = B\kappa^2/2$ where B is the local bending modulus and κ is the local curvature. The Frenet-Serret theorem gives $\kappa^2 = R^2[\theta'^4 + \theta''^2] + z''^2$, where the filament is parameterized by $\vec{r} = (R\cos\theta, R\sin\theta, z)$, both $\theta(s)$ and $z(s)$ depend on the arclength s, and primes indicate derivatives with respect to s. The inextensibility constraint is $1 = R^2\theta'^2 + z'^2$, which we implement with a Lagrange multiplier $\lambda(s)$, together with applied axial force density $f(s)$ and azimuthal force density $\tau(s)$, in a total energy $H = \int_0^L \mathcal{H}(s)ds$ where

$$\mathcal{H} \equiv \mathcal{H}_0 - R\theta\tau(s) - zf(s) - \lambda(R^2\theta'^2 + z'^2 - 1). \quad (2)$$

The problem is to find $\theta(s)$ and $z(s)$ that minimize H, such that $\delta\int_0^L \mathcal{H}ds = 0$. In general, this occurs when $\partial\mathcal{H}/\partial z - (\partial\mathcal{H}/\partial z')' + (\partial\mathcal{H}/\partial z'')'' = 0$ and the boundary conditions $\partial\mathcal{H}/\partial z' - (\partial\mathcal{H}/\partial z'')' = 0$ and $\partial\mathcal{H}/\partial z'' = 0$ are satisfied at $s = 0$ and $s = L$; and also equivalent equations for θ. For a static solution there must also be no net torque $\int\tau(s)ds = 0$ and no net force $\int f(s)ds = 0$.

Integrating the resulting equations once, scaling all lengths by the bacterial radius R so that the scaled arclength is $\tilde{s} \equiv s/R$ and the scaled filament length is $\alpha \equiv L/R$, and using $Z \equiv z'$ and $T \equiv \theta'$, we then have

$$Z'' + \tilde{\lambda}Z + Z'B'/B = F(\tilde{s}) \quad (3)$$

$$T'' - 2T^3 + \tilde{\lambda}T + T'B'/B = N(\tilde{s}) \quad (4)$$

$$Z^2 + T^2 = 1, \quad (5)$$

where the boundary conditions reduce to $Z' = T' = 0$ at $\tilde{s} = 0$ and $\tilde{s} = \alpha$. The scaled integrated axial force is $F(\tilde{s}) \equiv R^2\int_0^{\tilde{s}R} f(\sigma)d\sigma/B(\tilde{s})$ and the scaled integrated azimuthal force is $N(\tilde{s}) \equiv R^2\int_0^{\tilde{s}R}\tau(\sigma)d\sigma/B(\tilde{s})$. The magnitude of scaled forces is set by $B/R^2 \approx 0.6$ pN. We can use derivatives of the inextensibility equation, Eq. (5), to solve explicitly for $\tilde{\lambda} = Z'^2 + T'^2 + 2T^4 + TN + ZF$. The set of equations, Eqs. (3)–(5), can be solved using standard relaxation techniques [23] starting from a uniform helix. For simplicity, we solve cases where $B = \text{const}$ ($B' = 0$). The variables Z and T are related to the local unscaled helical pitch p,

$$p = 2\pi RZ/T = 2\pi RZ/\sqrt{1 - Z^2}, \quad (6)$$

which for a perfect helix is the axial distance over which the helix wraps once around the cylinder. Since p diverges for straight filaments (which are longitudinal, aligned with the cell axis), we will instead discuss Z which equals ± 1 for straight filaments and 0 for rings.

In the absence of external forces, with $F = N = 0$, Eqs. (3)–(5) only admit transverse loops with $T = 1$ and $Z = 0$ or short longitudinal filaments with $Z = 1$ and $T = \tilde{\lambda} = 0$. Perfect helices correspond to the vanishing of all derivatives of Z and T and so require *constant* F and N along the filament, i.e., delta-function forces at the filament tips. When both tip torques and tip forces are nonzero, then a perfect helix solution exists and satisfies $F = (N + 2T^3)Z/T$. For tip torques only, $F = 0$, we either have $\tilde{\lambda} = 0$ and a helix with $T = -(N/2)^{1/3}$ and $Z = \pm\sqrt{1 - (N/2)^{2/3}}$ or a ring with $Z = 0$ and $T = 1$. By considering H, we find that the helix is stable (minimal energy) below a critical torque of $N^* = 2$, above which the ring is stable. The bifurcation diagram is shown in the inset of Fig. 1. For axial tip forces only, $N = 0$, we either have a straight filament with $T = 0$ and $Z = \pm 1$, or

$$F = 2Z(1 - Z^2). \quad (7)$$

Above a critical compressive axial force, $F^* = 4/(3\sqrt{3}) \approx 0.77$, the helix is unstable and will snap over and align itself with the cylinder axis such that the axial forces become tensile. The smallest stable $|Z|$ is $Z^* = 1/\sqrt{3}$, corresponding to a *maximal* pitch $p^* = \pi\sqrt{2}R$. The bifurcation diagram is shown in Fig. 1, where we have shaded the experimental range seen for MreB homologs *in vivo*: from Mbl helices in *B. subtilis* with $|Z| \approx 0.56$ [4] to MreB rings in *E. coli* with $Z \approx 0$ [13]. The experimental range is inconsistent with fixed-magnitude axial tip forces only. Nonzero azimuthal forces, or torques, are required to explain experimentally observed helices.

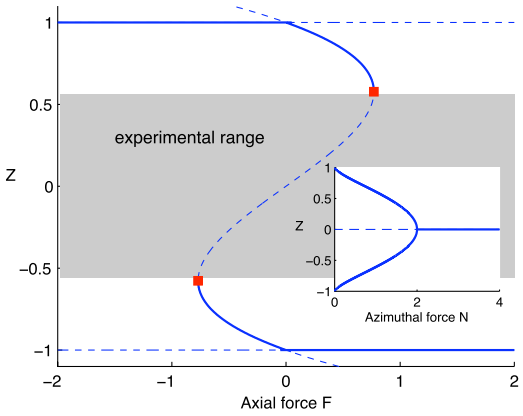

FIG. 1 (color online). Bifurcation diagram showing perfect helices with $Z \equiv z'$ vs scaled axial force F at filament tips. Stable branches are solid lines, unstable branches are dashed. Red squares are at the critical points $\pm(F^*, Z^*) = \pm[4/(3\sqrt{3}), 1/\sqrt{3}]$. The experimental range of Z observed for MreB homologs is indicated by the shaded region. The inset shows the bifurcation diagram for Z vs scaled azimuthal force N.

Forces that naturally act with respect to the filament orientation (i.e., in the Frenet frame), as well as static pinning forces, can be straightforwardly included in the numerical solution of the elastic equations through $\tau(s)$ and $f(s)$ determined self-consistently by the filament configuration. For example, constant $\tau(s)$ will generally resolve into nonconstant normal and tangential force densities in the Frenet frame. Here, we consider only simple force densities in the fixed bacterial frame.

Inhomogeneous helical pitches, such as observed with MreB in *E. coli* [13] are inconsistent with only tip forces and torques, but arise naturally from distributed forces along the filament length. We illustrate the effects of distributed forces by considering uniformly distributed azimuthal forces, where a constant torque density $\tau = N_0 B/(\alpha R^3)$ is applied everywhere along the filament along with a counterforce of magnitude N_0 at $\tilde{s} = \alpha$,

$$N(\tilde{s}) = N_0 \tilde{s}/\alpha - N_0 \delta(\tilde{s} - \alpha). \tag{8}$$

Other distributed azimuthal forces (e.g., linearly distributed [24]) give similar results. The resulting Z vs s/L are shown in Fig. 2(a) for a variety of N and a fixed filament length $\alpha = 20$ [25]. We see the boundary condition $Z' = 0$ at $s = 0$ and $s = L$, and the emergence of a ringlike structure ($Z \approx 0$) for larger s when $N > N^* = 2$, as illustrated by the real-space helical configuration for $N = 3$ [26]. While it would be difficult to systematically control $\tau(s)$ experimentally, N is scaled by the bending modulus B and so should be accessible by controlling the expression of the polymeric protein (i.e., MreB).

In Fig. 2(b) we show Z vs s/L for a fixed total force $N = 3$ and a variety of filament lengths. The $\alpha \to \infty$ limit, shown by a thick red (light gray) curve, corresponds to vanishing spatial derivatives in Eqs. (3) and (4)—the helical pitch is then determined by the instantaneous F and N. Note that $Z' \neq 0$ at $s = 0$ for this limit, which reflects a boundary layer that vanishes as $\alpha \to \infty$. The right inset shows that the width of this boundary region is $\Delta s \sim R$, less than one helical turn. (Comparing the solid $\alpha = 20$ and the dashed $\alpha = \infty$ curves in Fig. 2(a) shows that the boundary region is not strongly force dependent.) Corrections for finite filament length are substantial when the filament length approaches the bacterial circumference ($\alpha = 2\pi$), but are primarily seen near $s = 0$ and at the transition to ring collapse when $N(\tilde{s}) = 2$ (here at $s/L = 0.5$).

In the limit of long filaments, the transition between open helical configurations and a ring (where $Z = 0$) is abrupt. The location of this transition s/L as a function of N is shown in Fig. 3 by the thick red line. For shorter filaments, the transition is smooth and is shifted towards larger $N(\tilde{s})$—as illustrated by the thinner (black) lines for various α. For filaments that are not long enough to make a helical turn, large enough forces will tilt the entire filament into a ringlike configuration.

Other mechanisms for helical filaments within bacteria have been proposed. We have shown that shooting filaments without intrinsic curvature in a random direction [2] leads to an overly wide distribution of pitches. To describe observed helical pitches of MreB in bacteria, such a shooting mechanism would need additional pitch-selection mechanisms. For elastic filaments, such a mechanism would also need membrane anchors to prevent subsequent relaxation towards smaller pitches (though nonpolymerized helices [27] would not). Conversely, an equilibrium mechanism for helices has also been proposed for intrinsically curved filaments twisted by anisotropic association with the membrane [11]. Complementing such an approach, in this Letter we have considered helical configurations of intrinsically-straight elastic filaments that are bent by applied and constraint forces without twist.

For elastic filaments without intrinsic curvature, such as MreB, we have shown how applied forces can lead to perfect helices (if forces are tip directed) or helices with

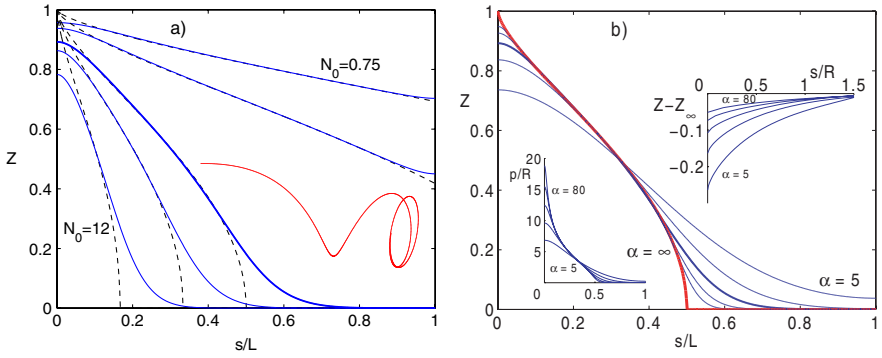

FIG. 2 (color online). Equilibrium configurations $Z \equiv z'$ vs $s/L = \tilde{s}/\alpha$ for uniformly distributed azimuthal forces $\tau(s)$ following Eq. (8). (a) Fixed scaled length $\alpha = 20$ and scaled azimuthal forces $N_0 = 0.75$, 1.5, 4, 6, and 12 [blue (dark gray) curves]. The real-space helical configuration for $N_0 = 3$ [medium-weight blue (dark gray) curve] is shown in red (light gray). The $\alpha = \infty$ limits for the same range of azimuthal forces are shown by black dashed lines. Significant α dependence is seen both at the free tip and at the transition to $Z = 0$. (b) Fixed azimuthal force $N_0 = 4$ and various scaled lengths $\alpha = 5$, 10, 20, 40, 80 [blue (dark gray) curves], and ∞ [thick red (light gray) curve]. The left inset shows the pitch distributions of the configurations with finite α. The right inset, plotting $Z_\alpha - Z_\infty$ vs s/R, shows that the boundary layer, near $s = 0$, has a width of order R.

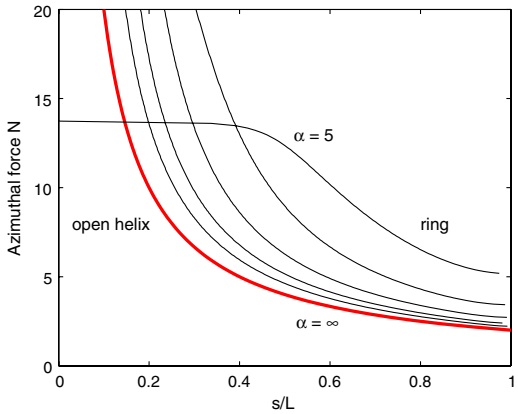

FIG. 3 (color online). In the limit of long filaments, with $\alpha = \infty$, the range of filament length s/L and scaled azimuthal force N that have rings ($Z = 0$) are shown above the thick red line, while open helical configurations are seen below the line. No rings are seen below $N^* = 2$. For shorter filaments, this phase diagram still applies approximately. Shown are the lines separating $Z < 0.01$ and $Z > 0.01$ for $\alpha = 5$, 10, 20, 40, and 80, using Eq. (8). For shorter filaments (as shown here for $\alpha = 5$), the entire short filament is ring-shaped at larger forces.

instantaneous pitches that vary along their length (if forces are distributed). We derive and solve the equations that describe the helical configurations that result. In particular, azimuthal forces in a physiological range (1–25 pN) can give rise to a helixlike configuration with a pitch in the experimentally observed range of MreB (0.5–2.0 μm). Distributed azimuthal forces result in the coexistance of extended helical and collapsed ringlike configurations in the same filament, as observed with MreB in *E. coli* [13]. When rings of MreB are observed in *E. coli* [13] the fluorescence intensity of the filament appears to diminish—which may indicate thinner filaments and correspondingly smaller B and larger $N(\tilde{s})$. Unbundling (or rebundling) MreB filaments may be an accessible switch to turn on (or off) ringlike collapse within bacteria.

Force generation within bacterial cells remains a frontier, with no reported homologs of the processive motors associated with cytoskeletal filaments in eukaryotic cells (e.g., dynein, myosin, kinesin). We have shown that azimuthal forces would be required for the helical configurations that are observed for MreB, and such forces are unlikely to simply result from geometric constraints. A detailed and quantitative study of inhomogeneous helical pitch and of bending modulus (potentially accessible via variations of fluorescence intensity along the filament) can now be used to access distributed azimuthal (and axial) forces distributed along the filament, and hence to explore active force generation within bacteria.

J. F. A. thanks Yoichiro Mori for advice on numerical methods. This work was supported financially by NSERC.

*URL: http://www.physics.dal.ca/~adr

[1] K. A. Michie and J. Lowe, Annu. Rev. Biochem. **75**, 467 (2006).
[2] Y.-L. Shih and L. I. Rothfield, Microbiol. Mol. Biol. Rev. **70**, 729 (2006).
[3] S. Thanedar and W. Margolin, Curr. Biol. **14**, 1167 (2004).
[4] L. J. F. Jones, R. Carballido-López, and J. Errington, Cell **104**, 913 (2001).
[5] Y.-L. Shih, T. Le, and L. I. Rothfield, Proc. Natl. Acad. Sci. U.S.A. **100**, 7865 (2003); G. Ebersbach and K. Gerdes, Mol. Microbiol. **52**, 385 (2004); A. Taghbalout and L. Rothfield, Proc. Natl. Acad. Sci. U.S.A. **104**, 1667 (2007).
[6] R. A. Daniel and J. Errington, Cell **113**, 767 (2003).
[7] J. H. Russell and K. C. Keiler, J. Bacteriol. **189**, 7581 (2007); PLoS ONE **3**, e1756 (2008); S. Lewenza, M. M. Mhlanga, and A. P. Pugsley, J. Bacteriol. **190**, 6119 (2008).
[8] N. Chouaieb, A. Goriely, and J. H. Maddocks, Proc. Natl. Acad. Sci. U.S.A. **103**, 9398 (2006).
[9] S. S. Andrews and A. P. Arkin, Biophys. J. **93**, 1872 (2007).
[10] H. P. Erickson *et al.*, Proc. Natl. Acad. Sci. U.S.A. **93**, 519 (1996); R. Srinivasan *et al.*, Genes Dev. **22**, 1741 (2008).
[11] R. Srinivasan *et al.*, Curr. Biol. **17**, 266 (2007).
[12] M. C. Lagomarsino *et al.*, Biophys. J. **92**, 1046 (2007).
[13] P. Vats and L. Rothfield, Proc. Natl. Acad. Sci. U.S.A. **104**, 17 795 (2007).
[14] R. Carballido-López, Microbiol. Mol. Biol. Rev. **70**, 888 (2006).
[15] T. Kruse, J. Bork-Jensen, and K. Gerdes, Mol. Microbiol. **55**, 78 (2005).
[16] O. Esue, D. Wirtz, and Y. Tseng, J. Bacteriol. **188**, 968 (2006).
[17] G. H. M. van der Heijden, Proc. R. Soc. A **457**, 695 (2001).
[18] T. Kruse *et al.*, Genes Dev. **20**, 113 (2006).
[19] W. Vollmer and J.-V. Höltje, Curr. Opin. Microbiol. **4**, 625 (2001).
[20] P. M. Slovak, S. L. Porter, and J. P. Armitage, J. Bacteriol. **188**, 1691 (2006); A. V. Divakaruni, C. Baida, C. L. White, and J. W. Gober, Mol. Microbiol. **66**, 174 (2007).
[21] J. F. Allard and A. D. Rutenberg, Phys. Rev. E **76**, 031916 (2007).
[22] H. J. Defeu Soufo and P. L. Graumann, EMBO J. **5**, 789 (2004); R. Carballido-López *et al.*, Dev. Cell **11**, 399 (2006).
[23] W. H. Press *et al.*, *Numerical Recipes: the Art of Scientific Computing* (Cambridge University Press, New York, 2007), 3rd ed..
[24] Motors binding at a fixed rate then advecting with the filament [21] would give a linear force distribution.
[25] $L/R = \alpha = 20$ allows for 2–3 complete windings of circumference $2\pi R$ along the filament length.
[26] Using $R \approx 400$ nm, $\int \tau \approx 1$ pN, and $B \approx 10^5$ pN nm^2, we obtain $N \approx 1.6$.
[27] One might "spray-paint" a new helix of pitch $p = p_0/[1 - \omega R v^{-1}\sqrt{1 + p^2/(2\pi R)^2}]$ from a locus treadmilling at speed v [21] along a preexisting helix of pitch p_0 that is itself rotating at an angular speed ω.